Journal of Power Sources 245 (2014) 345–351

Contents lists available at SciVerse ScienceDirect

Journal of Power Sources

journal homepage: www.elsevier.com/locate/jpowsour

# Nanotin alloys supported by multiwall carbon nanotubes as high-capacity and safer anode materials for EV lithium batteries

S. Menkin [a], Z. Barkay [b], D. Golodnitsky [a,b,*], E. Peled [a]

[a] School of Chemistry, Tel Aviv University, Tel Aviv 69978, Israel
[b] Wolfson Applied Materials Research Center, Tel Aviv University, Tel Aviv 69978, Israel

## HIGHLIGHTS

- Synthesis and characterization of nanotin powders supported by multiwall carbon nanotubes.
- Modified electroless deposition.
- Prolonged cycle life.

## ARTICLE INFO

*Article history:*
Received 22 March 2013
Received in revised form
6 June 2013
Accepted 21 June 2013
Available online 1 July 2013

*Keywords:*
Li-ion battery
Electroless
Tin alloy
Carbon nanotubes

## ABSTRACT

Much effort has been expended in the search for new lithium-containing anode materials. Alloy anodes based on tin are known for their high specific capacity and safety characteristics. The theoretical specific capacities of alloy anodes are 2–10 times that of graphite. The second merit of alloy anodes is their moderate operation potential versus lithium. For example, Sn anodes have an onset-voltage potential of 0.6 V above that of $Li/Li^{+}$. This moderate potential averts the danger of lithium deposition which is present in the case of graphite anodes (~0.05 V vs. Li).

This study is directed to the synthesis and characterization of nanotin powders supported by multiwall carbon nanotubes (MWCNT). Modified electroless deposition (ELD) was used for the preparation of high-surface area tin-alloy nanosized anodes. In this work, it was found that the use of nanoparticles of tin deposited on multiwall carbon nanotubes, enables prolonged cycling of a tin-composite anode in a lithium-ion battery.



## 1. Introduction

Despite the technologically advanced nature of modern industries, each can be brought to a grinding halt by an event that lasts less than 1 s. Because the majority of power-quality events are short, the most likely choice for combating the problem is energy storage. Energy-storage technologies have made great strides in recent years and now offer a variety of choices for ride-through power, proving that although simple in concept, batteries can provide a reliable solution to a complex problem.

There are several evolving markets for energy storage. Two of them require large, long-life (several thousands of cycles), safe and low-cost batteries. These are the power-quality and digital-reliability market, where the batteries bridge outages seamlessly, and the electric-vehicles (EV) market. In the first market, the high-temperature sodium–sulfur battery dominates (sales of over $100M per year) and the best candidate for the second market is the lithium-ion battery. High battery cost, low anode capacity and unsatisfactory anode safety are obstacles that must be overcome in order to enable commercialization of the large lithium-ion battery for these applications. At present, lithium-ion batteries are not sufficiently safe, are too expensive and have too short a cycle life. The graphite anode is the source of some hazardous incidents.

Alloy anodes based on tin are known for their high specific capacity and their safety characteristics. The theoretical specific capacities of alloy anodes are 2–10 times that of graphite. Even if the full volume expansion of lithiated products is considered, the charge densities of alloy anodes are still 2–5 times that of graphite. For example, the lithium–tin alloy, in its fully lithiated composition, $Li_{4.4}Sn$, has a theoretical specific capacity of 994 mAh $g^{-1}$, namely, a value almost three times that of conventional graphite (372 mAh $g^{-1}$). The second merit of alloy anodes is their moderate

* Corresponding author. School of Chemistry, Tel Aviv University, Tel Aviv 69978, Israel.
*E-mail addresses:* dgolodnitsky@gmail.com, golod@post.tau.ac.il (D. Golodnitsky).

0378-7753/$ – see front matter © 2013 Elsevier B.V. All rights reserved.
http://dx.doi.org/10.1016/j.jpowsour.2013.06.131

operation potential versus lithium. For example, Sn anodes have an onset voltage of 0.6 V above Li/Li+. This moderate potential averts the danger of lithium deposition as occurs with graphite anodes (~0.05 V vs. $Li/Li^+$).

The main challenge to the implementation of alloy anodes is their large volume change (up to 320%) during lithium insertion and extraction, which often leads to pulverization of the active alloy particles and poor cycle stability. In addition, the first-cycle irreversible capacity loss of alloy anodes is too high [1,3]. Extensive research has been carried out to address these two issues and significant progress has been made during the last two decades [2–22].

In an attempt to reduce the fall in reversible capacity and the first-cycle irreversible capacity of alloy anodes, several strategies have been developed. The major effort has been focused on reducing the detrimental effects of large volume changes and on alleviating the side reaction with the electrolyte. The main strategy is a combination of a host matrix to buffer the large volume change of the active particles and reduction of the particle size to the nanometric scale. However, the large surface area of the nanoparticles increases the side-reactions and SEI formation, which may lead to self-discharge, poor cycling life and short calendar life. One possible way to overcome these problems is to prepare anode composites comprising large primary particles and secondary nanoparticles [1].

Carbon nanotubes (CNTs) have extraordinary thermal and mechanical stability and high electronic conductivity, which makes them an ideal candidate for nanoscale matrix material for the lithium-alloying metal [23]. According to the DFT model of Zheng et al., the tailoring of tin nanoparticles does not impair the high conductivity of CNTs; in fact, the Sn nanoparticles attached to the CNT provide metallic conductivity to the system. In addition, according to Zheng's model, tin clusters have an adsorption energy much smaller than that of a single Sn atom. The model also indicates that the energy of adsorption to the outer surface of the CNT is about 2–3 times that of adsorption to the inner surface. Consequently, the formation of discrete metal particles on the outer surface of the CNT is preferred. Many elements are reactive towards lithium; however, only Si, Sn, Sb, Al and Mg have been widely investigated since they are cheap, abundant and environmentally friendly. In 2005, Sony began marketing "Nexelion", a new type of Li-ion battery, the first commercial battery with tin-based anode. According to Inoue and Wolfenstine [24,25], the "Nexelion" anode consist mainly of 27%(w/w) tin, 16%(w/w) cobalt and 36%(w/w) carbon. The use of a tin-alloy anode and a modified cathode, gives the Nexelion cell several advantages over the conventional Li-ion cell. These include: 30% increase in capacity, 20% increase in power, 20% increase in volumetric energy density, 10% increase in weight energy density, quicker charging times at room temperature (20% increase in charge efficiency), improved charge and discharge performance at low temperatures (40% increase in discharge capacity at −20 °C) and better thermal stability.

During the last ten years, tin oxide–CNT, tin alloy–CNT and tin–CNT composite anodes have been studied [26–34]. For example, Noerochim et al. [34] prepared a $SnO_2$-coated MWCNT composite anode by a hydrothermal method and obtained 473 mAh $g^{-1}$ and 50% capacity retention at cycle 100. Lee [27] prepared an SWCNT/tin nanoparticle composite by electrochemical reduction and obtained 535 mAh $g^{-1}$ and 76% capacity retention at cycle 50.

In this study, the preparation of tin alloys by electroless deposition (ELSD) was chosen since, in addition to all the above advantages, there is an established technology for the ELSD of tin in the electronics industry [28–34]. Tin-based anode material supported by multiwall carbon nanotubes, Sn-MWCNT, was synthesized by a multistep electroless deposition process. First, a tin–copper alloy, $Sn_xCu_y$, was formed on the carbon nanotubes. The preparation process for the anode material, $Sn_xCu_y$-MWCNT, consists of two main stages: the electroless deposition of copper nanoparticles on activated MWCNT and the coating of tin over the copper nanoparticles by replacement deposition. The result is core(Cu)–shell(Sn)-structured particles. The role of the inert metal (copper) in this structure is to strengthen the structure during the processes of expansion and contraction on repeated cycling of the anode. This stabilizes the anode structure even more than does the MWCNT matrix alone. In later stages of the research it was established that it is sufficient to stabilize the tin particles by the carbon nanotubes, which provide improvement of the specific capacity of the anode on prolonged cycling.

## 2. Experimental

Extensive research has been conducted on the issue of the dispersion and activation of carbon nanotubes [18,28,35,36]. Because of the strongly hydrophobic and inert character of the MWCNTs, it is essential to activate their surface in order to create hydroxide and carboxylic surface groups prior to MWCNT-Sn bonding. MWCNT powder (SkySpring) was activated by treatment in a mixture of acids. For the purpose of activation, a solution of 0.25–0.5%(w/v) MWCNT in 3:1(v/v) $H_2SO_4$ (98%(w/w)):$HNO_3$ (70%(w/w)) was stirred for 10–12 h.

Fig. 1 shows an ESEM image of MWCNT before (left) and after (right) pretreatment. A comparison of the images shows that the pretreatment makes the MWCNTs more dispersed and shorter. Analysis of the XPS spectra of tubes before and after pretreatment (not shown here) revealed that the acid activation causes oxidation of the MWCNTs and creation of C=O, OH–C=O and C–O surface groups.

The activated MWCNT sample was placed in 0.13 M $SnCl_2$ aqueous solution and stirred for about 30 min. This step enables adsorption of $Sn^{2+}$ cations on the surface of the carbon nanotubes. Then the sample was placed in 200 ml 2.3 mM $PdCl_2$ solution under continuous stirring for 30 min. The powder was rinsed with distilled water after each step. $Pd^{2+}$ is reduced by the adsorbed tin cations to form the nucleus of Pd on the tubes.

The deposition of tin nanoparticles on the activated-carbon nanotubes was conducted by two electroless methods: conversion coating of tin on a seed copper layer and modified direct tin coating.

### 2.1. Cu electroless seed-layer deposition (Cu ELSD)

An aqueous solution of $CuSO_4 \cdot 5H_2O$ (35 g $l^{-1}$) and $Na_2EDTA$ (50 g $l^{-1}$) was prepared; the pH was adjusted to 11.5–12.5 and formaldehyde was added to a concentration of 10 g $l^{-1}$. The Cu ELSD lasted 3 h under continuous stirring at 70–75 °C.

### 2.2. Sn conversion coating

A tin-conversion coating bath based on a recipe described in Ref. [28] was used. The bath consisted of 0.3 M $SnCl_2$ as the source of tin, 0.65 M $Na_3C_6H_5O_7$ as the complexing agent, 1.5 M $(NH_2)_2CS$ and 0.35 M $NaH_2PO_4 \cdot H_2O$ as the reducing agent. The pH of the EDSL bath was about 5 and the temperature was kept at 75–83 °C during the 2- to 4-h process. The process was carried out under nitrogen atmosphere in order to prevent oxidation of metallic tin. The resulting powder was washed thoroughly with distilled water, until chlorides were not found by the $AgNO_3$ test. The powder was dried at 100 °C under vacuum.

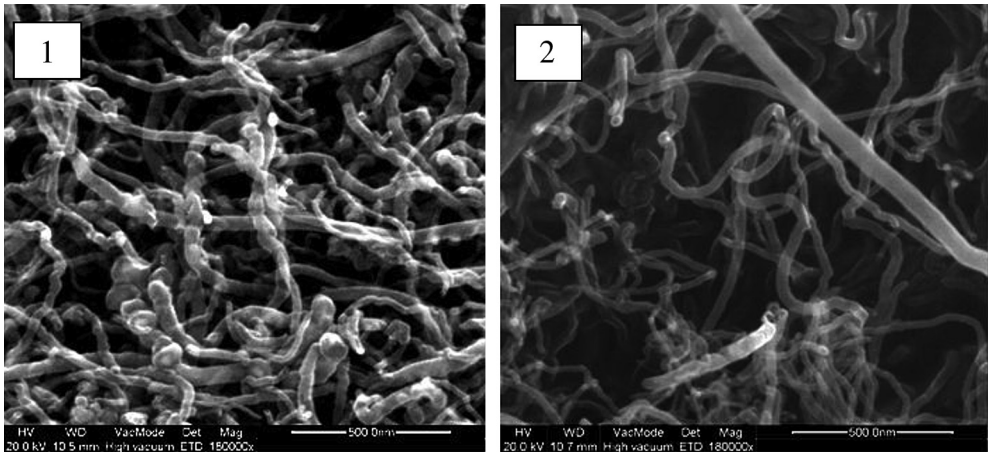


**Fig. 1.** ESEM image of MWCNT before (1) and after (2) pretreatment in the mixture of acids.

### *2.3. Preparation of nanotin alloy anode by direct electrochemical reduction on MWCNT*

The bath for the direct ELSD of tin contained: 0.3 M $SnCl_2 \cdot 2H_2O$, 0.40M HCl, 0.47 M $NaH_2PO_2 \cdot H_2O$ and 0.65 M $Na_3C_6H_5O_7 \cdot 2H_2O$. The process of electroless reduction of tin lasted 4–5 h and as mentioned above, was carried out under nitrogen atmosphere. After washing, the powder was dried at 100 °C under vacuum.

### *2.4. Preparation of the anodes*

A slurry of 10–15%(w/w) (from the solids) PVDF (Kynar) and 85–90% MWCNT-Sn or MWCNT-SnCu was prepared. The slurry was spread on a copper current collector to achieve loading of 0.5–5 mg $cm^{-2}$. The anodes were dried for 2–3 h under vacuum at 100 °C.

Coin cells of the MWCNT-Sn anode vs. lithium metal (FMC) were assembled with 1 M $LiPF_6$ EC:DEC 1:1 electrolyte (Ferro). The cells

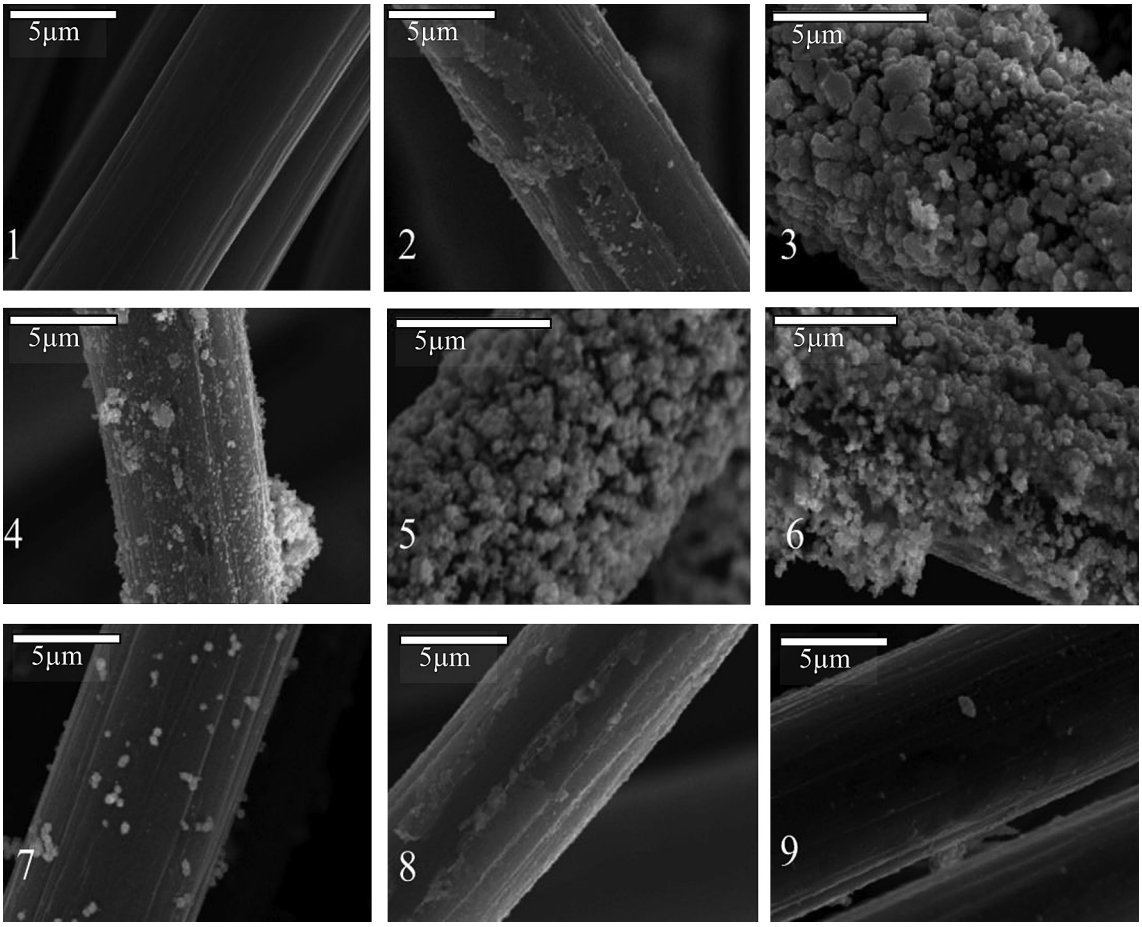


**Fig. 2.** SEM micrographs of copper coating deposited by electroless method on charcoal carbon fiber cloth at different deposition-bath parameters. The samples were prepared in the electrolyte with 1:1 $[Cu^{2+}]$: $[C_6H_{12}N_2(COO)_4]^{4-}$ ratio. Deposition time 15 min. The ratio of $CH_2O$ to $Cu^{2+}$ is: 3.6:1 (samples 2–6); 5.4:1 (sample 7); 7.2:1 (sample 8), Pristine fibre (sample 1); pH11, 60 °C (sample 2); pH13, 60 °C (sample 3); pH12 60 °C (sample 4); pH12, 70 °C (samples 5, 7–9); pH12, 80 °C (sample 6).

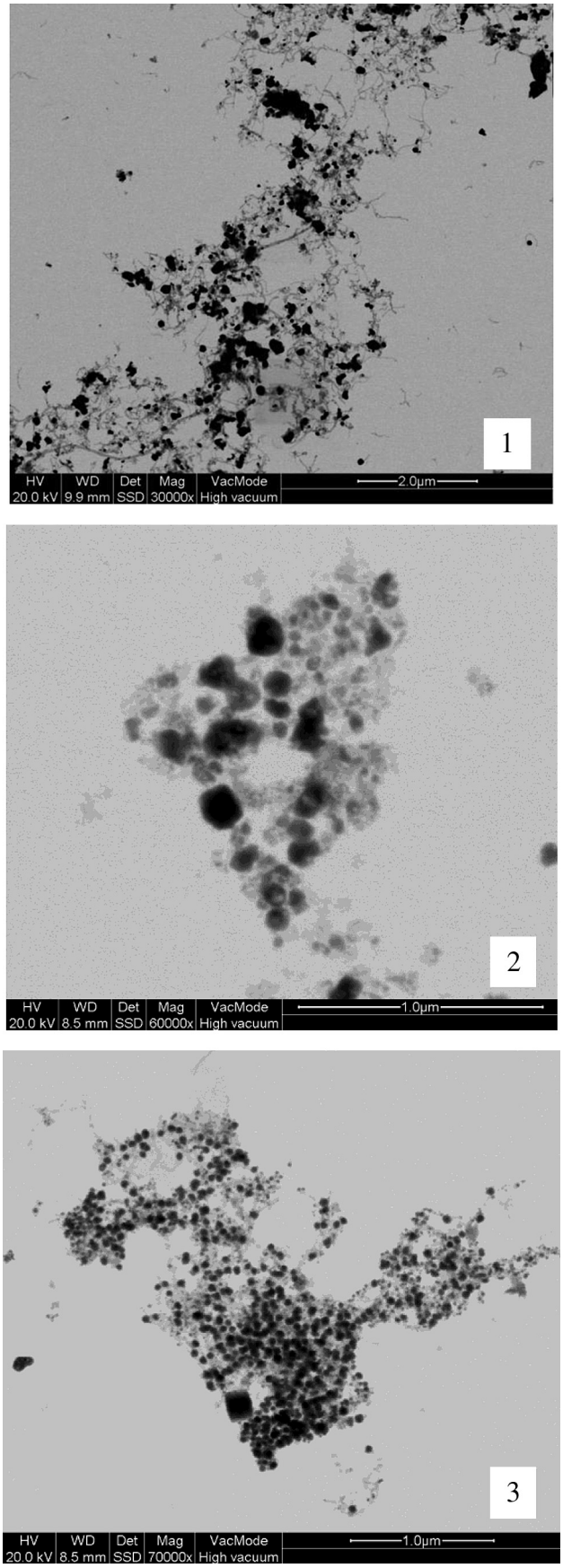


**Fig. 3.** BF-STEM images of tin–copper-coated MWCNT samples. Deposition of underlying copper carried out for 2 h at pH = 12 and 75 °C (sample 1); 1.5 h (sample 2); in diluted copper bath for 3 h at pH 10.5 and 70 °C sample 3.

were cycled at a current density of 0.03–0.1 mA $cm^{-2}$ over the potential window of 0.05–1.2 V.

The tin concentration in the cycled electrodes was determined by a UV/visible spectrophotometric technique [37]. For this purpose, the Li/Sn-MWCNT cell was disassembled after cycling. The Sn-MWCNT electrode was dissolved in acetone in order to separate the active material from the copper current collector and the acetone was removed by evaporation. The tin from the remained powder was dissolved in hot concentrated sulfuric acid with stirring for a few hours. To promote complete dissolution and oxidation of tin, the anode was kept in acid at RT overnight. The final suspension was diluted and filtered through filter paper. The tin content was determined by spectrophotometric measurement of the absorbance of the complex of tin (IV) with bromopyrogallol (BPR) at $\lambda = 304$ nm.

The preparation of the samples for STEM analysis was carried out in a similar manner. After the dissolution of the cycled anode in acetone, a sample of Sn-MWCNT particles was transferred to ethanol and dispersed by ultrasonication. The TEM grid was dipped into the resulting solution and the solvent was evaporated.

Anode-particle size and distribution were determined by simultaneous STEM (scanning transmission electron microscopy) and SE (secondary-electron) microscopy by the Quanta 200FEG ESEM. High-resolution transmission electron microscopy (TEM) was carried out by a Tecnai F20 (FEI) with a 200 kV field-emission gun. XPS analysis was performed with a Philips UHV-5600 apparatus with an AlK_emission source.

## 3. Results and discussion

The tin content of the anode material should be high enough to achieve specific capacity higher than that of the graphite-based anode. In the current study, our aim was to create high-loading anodes composed of separated nanoparticles of tin attached to the carbon nanotubes. Small, separated tin particles attached to the rigid, high-conducting matrix of nanotubes is expected to eliminate merging of the nanoparticles during volume expansion, caused by anode lithiation during battery charge, and pulverization of the active material during cycling.

The deposition of tin nanoparticles on the activated-carbon nanotubes was conducted by two electroless methods: conversion coating and modified direct coating. For the conversion coating, copper nanoparticles were deposited as a seed layer on the palladium-activated MWCNT. Then the copper nanoparticles were exchanged by tin via the displacement reaction. In order to select the optimal parameters of synthesis of the copper seed layer, samples of charcoal carbon cloth (Etek) were used. The cloth is made up of 10 μm-diameter carbon fibers, which mimic the nanotubes. This method provides a quick overview of the different coating conditions, since there is no need for a complex pretreatment of the nanotubes to prevent their entanglement. In addition, a routine SEM characterization method is sufficient as compared to complex STEM tests of the MWCNTs.

The carbon fibers were coated by a seed copper layer in electrolytes with different pH, temperature and relative concentrations of the electrolyte components. The SEM micrographs (Fig. 2) show that electroless deposition at pH 13 causes vigorous growth of large spheroid-shaped 0.5–2-μm size particles and non-uniform coating of the carbon-cloth fiber. The deposit at pH 12 is more homogeneous – composed of 1-μm size particles, with few clusters; at pH

**Table 1**
Chemical composition of the MWCNT-$Cu_xSn_y$ anodes.

| Compound (w/w %)/sample number | 1 | 3 | 4 |
|---|---|---|---|
| Sn | 8 | 20 | 38 |
| Cu | 1 | 3 | 0.3 |
| C | 56 | 48 | 38.7 |
| O | 23 | 19 | 19 |
| F (from PVDF) | 13 | 10 | 4 |
| Sn:Cu weight ratio | 8:1 | 7:1 | 112:1 |
| Sn:$SnO_2$ weight ratio | 0.21 | [a] | 0.28 |

[a] High-resolution test was not done.

**Table 2**
XPS data for electrodes based on anode material sample 4 and PVDF binder, for different sputtering times.

| Sputtering duration (depth)/element weight % by XPS | 0 min (surface composition) | 2 min (8 nm depth) | 6 min (16 nm depth) | 10 min (39 nm depth) |
|---|---|---|---|---|
| C | 38.45 | 40.00 | 38.08 | 36.79 |
| O | 18.90 | 7.72 | 3.23 | 1.20 |
| Sn | 38.27 | 43.22 | 47.45 | 47.70 |
| Cu | 0.34 | 3.70 | 5.64 | 7.78 |
| F | 4.04 | 3.04 | 2.41 | 3.46 |
| Pd | 0 | 2.30 | 3.20 | 3.07 |
| Sn:Cu atomic ratio | 0 | 6.2:1 | 4.5:1 | 3.3:1 |

11 the coating of the fibers is non-continuous. The reduction process is very slow at temperatures below 70 °C. Increasing the concentration of the reducing agent (formaldehyde) relative to the $Cu^{2+}$ content of the solution, suppresses the growth of large grains, but leads to thinner layers. On the basis of these experiments, the optimal parameters for the deposition of the copper seed layer were selected as follows: pH 12, 75 °C and ratio of reducing agent-to-copper ion concentrations 3.6:1.

ELSD of tin onto copper-coated MWCNTs was carried out as described in Section 2. However, it appeared that the optimized parameters for the ELSD of copper on the fiber cloth were not completely suitable for the nanotubes. Bright-field STEM images (Fig. 3) show the morphology of MWCNT-supported tin nanoparticles deposited on a copper seed layer prepared in the solutions with constant $Cu^{2+}$:$Na_2EDTA$ ratio and at pH 12. Palladium activation of the tubes was carried out and we found that the longer the palladium activation, the more nucleation sites were created and the smaller the final tin particles. No significant difference was detected between the influence of ultrasonic and magnetic stirring of the solution on the particle size. Sample 1 was prepared by tin coating of copper deposited on activated MWCNT for 2 h in an electrolyte containing 1.67 mol of formaldehyde at pH = 12 and 75 °C with constant magnetic stirring. The size of the tin particles was about 150 nm. When the deposition time for the underlying copper was reduced to 1.5 h (the second sample), the size of the tin particles was similar − 130 nm (sample 2). Dilution of the copper electrolyte by a factor of two and lowering of the pH to 10.5 and the temperature to 70 °C promote better dispersion of the carbon nanotubes, smaller tin particles (53 nm) and their more homogeneous distribution on the surface (sample 3); this, despite the longer duration (3 h) of the Cu ELSD process.

The duration of the copper coating of sample 4 (Table 1) is half that of sample 1; the concentration of $Cu^{2+}$ in the electrolyte is one third that of sample 1; the tin-bath composition and operating conditions are the same.

Table 1 summarizes the results of the XPS surface analysis of the $Sn_xCu_y$-MWCNT samples.

According to the XPS tests, the chemical composition of the surface of sample 4 (Table 1) is 38% tin, 0.3% copper, 38% carbon, 19% oxygen and 4% fluorine. As can be seen from Table 1, the highest efficiency of copper displacement by tin and the most uniform distribution of tin nanoparticles on the MWCNT surface was achieved in sample 4, where the $Cu^{2+}$ concentration in the electrolyte was significantly reduced. We believe that this is related to the formation of a large number of small copper nuclei, which in turn induce simultaneous reduction of $Sn^{2+}$ and produce tin nanocrystallites. Anodes composed of $Sn_xCu_y$-MWCNTs (sample 4) and PVDF were fabricated.

Table 2 shows the results of the XPS analysis of the surface and bulk of the anodes.

As is evident from the table, the surface concentration of copper in $Sn_xCu_y$-MWCNT anodes is negligible. Increasing copper concentration in the bulk indicates incomplete displacement of copper by tin. The presence of palladium in the bulk shows that not all the activation sites have been used for the reduction of copper. High oxygen content before sputtering indicates that the tin nanoparticles are covered by a layer of oxide. On the basis of the data obtained so far, we believe that the electroless reduction of $Sn^{2+}$ may occur in parallel with the tin-copper conversion reaction. According to the SEM-EDS results, only 67% of the copper was converted by tin, with 33% remaining as copper metal in the anode material. Since copper is not an active anode material in the lithium-ion battery, and since its contribution to the mass of the

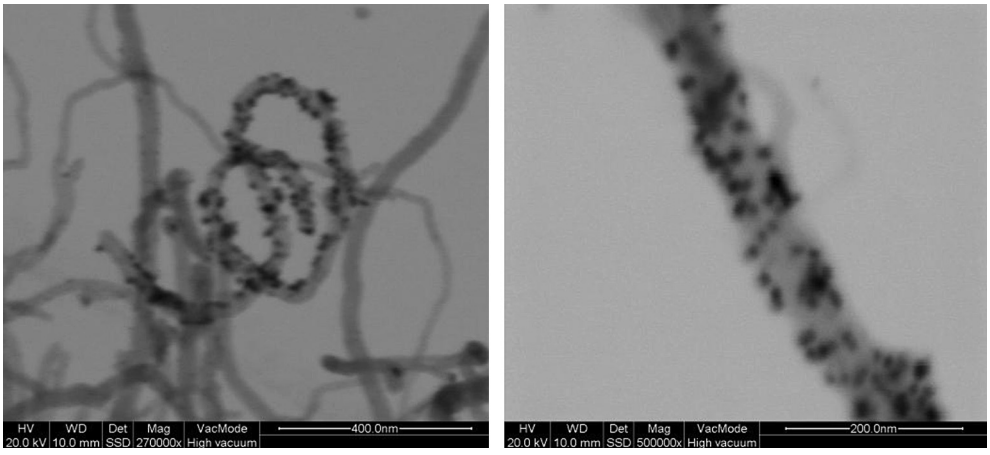


**Fig. 4.** Tin nanoparticles deposited on Pd-activated MWCNTs at pH5 and 75 °C at different magnifications.

anode is four times that of carbon, the remaining copper is disadvantageous ballast.

In the second approach, an attempt was made to carry out direct electroless deposition of tin on carbon nanotubes, without the plating of a copper seed layer. The conversion-coating tin bath developed by Ref. [28] and the ELSD tin bath [30] are very similar; they both contain a tin salt, complexing and reducing agents. The baths differ only in the concentrations of the electrolyte components. The conversion-coating bath is one order of magnitude more concentrated than the ELSD bath. As the MWCNT-supported anode material is a high-surface area powder, we preferred using the content of the conversion-coating bath for the direct ELSD of tin.

Carrying out the tin ELSD on Pd-activated MWCNTs under the optimized conditions (pH 5, 75 °C), yields homogeneous covering of the MWCNT by well dispersed tin nanoparticles of about 6–14 nm diameter (Fig. 4). The resulting anode-material powder contains about 40%(w/w) tin (estimated by SEM-EDS). According to the HR-XPS tests of the anode, spread on a copper current collector, the anode contains about 29%(w/w) tin. It was found that 27% of the tin is in metallic form and 73% is oxide.

Fig. 5 shows the cycleability plot of the Li/LiPF$_6$ EC:DEC/$Sn_{70}Cu_{30}$ cell. In order to additionally stabilize the anode structure, an artificial SEI (ARTSEI) layer was created on top of the anode by casting an aqueous solution of 0.5%(w/w) sodium carboxymethylcellulose and vacuum-drying at 100 °C. The capacity of the first lithium-alloying step was 900 mAh g$^{-1}$ Sn. The irreversible capacity of the cell was 27%. During the first 20 cycles the cell lost 26% of its initial reversible capacity. However, after that, significant stabilization of the electrochemical behavior was observed. The capacity-retention rate during the following 80 cycles was 0.7%/cycle.

The voltage profile of the lithium cell with MWCNT-supported tin anodes, prepared by direct ELSD, is presented in Fig. 6. The profile is typical for a tin anode with the tin-lithium alloying over the 0.4–0.8 V range.

The MWCNT-supported tin anodes prepared by direct ELSD have capacities of about 530–900 mAh g$^{-1}$ Sn, corrected for the carbon contribution. It was found that thick electrodes with 2.5 mg cm$^{-2}$ loading have capacities of 530–600 mAh g$^{-1}$ and very stable cycle life (degradation rate of 0.1% per cycle). Li/Sn-MWCNT cells with thick anodes retain 71% of their initial reversible capacity

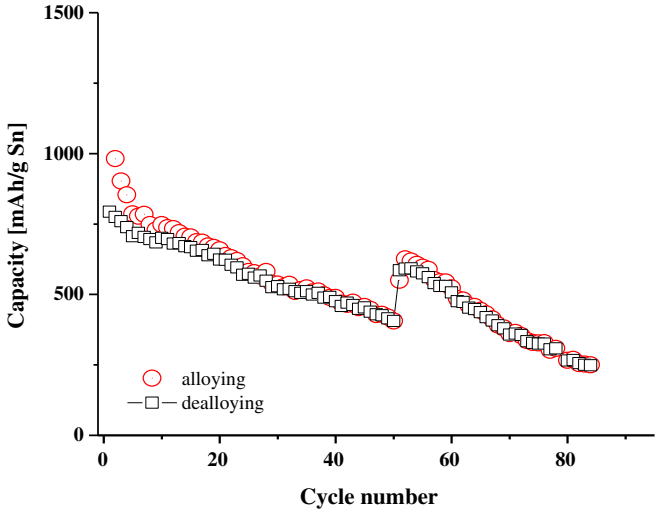


**Fig. 5.** The cycleability plot of the Li/LiPF$_6$ EC:DEC/$Sn_{70}Cu_{30}$ cell, $i_d = i_{ch} = 0.3$ mA cm$^{-2}$ until cycle 50, $i_d = i_{ch} = 0.1$ mA cm$^{-2}$ from cycle 51.

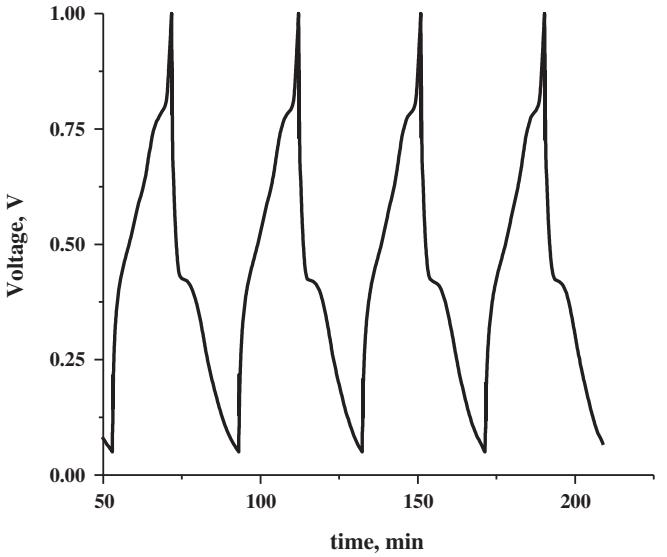


**Fig. 6.** Charge/discharge voltage profiles of Li/LiPF$_6$ EC:DEC/Sn-MWCNT cell, $i_d = i_{ch} = 0.3$ mA cm$^{-2}$.

at cycle number 280 (Fig. 7). High irreversible capacity is caused by the formation of a solid electrolyte interphase film and severe surface oxidation, as found by the XPS tests. We would like to mention, however, that while 73% of the tin is in the oxide form, it appeared that about 30% of the oxidized tin is reduced during the first few cycles and is utilized as active material in the cell. Insufficiently high-capacity values may be due to slow diffusion in the bulk materials. The cells with thin anodes of about 1.5 mg cm$^{-2}$ loading, show very high capacity (about 900 mAh g$^{-1}$ Sn), but shorter cycle life.

The effect of cycling on the size, shape and location of tin particles was tested by STEM. In Fig. 8, dark-field STEM images of a pristine and cycled Sn-MWCNT anode (in the charged state) are presented. On the basis of the statistical analysis carrying out on many STEM images, the average tin particle size in the pristine Sn-MWCNT anode was 10 ± 4 nm. After 179 cycles, the size of the particle increased to 15 ± 6 nm. It seems likely that, although the particle size increased by 50%, the Sn-MWCNT anode preserved its structure. The PVDF binder of the anode masks the bundles of nanotubes, which

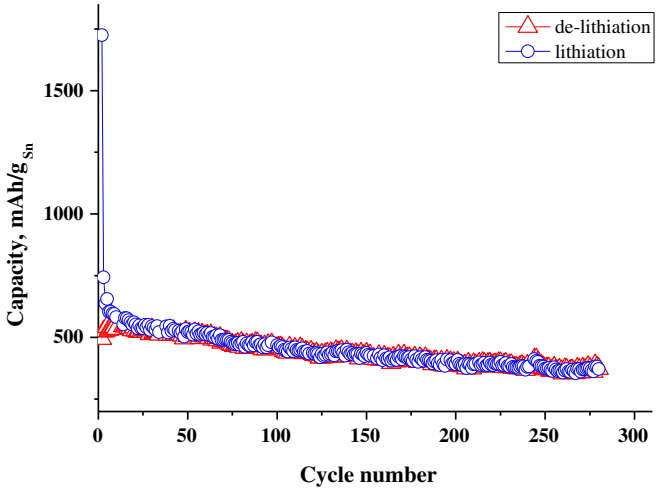


**Fig. 7.** Cycle life of Li/LiPF$_6$ EC:DEC/Sn-MWCNT cell, $i_d = i_{ch} = 0.3$ mA cm$^{-2}$.

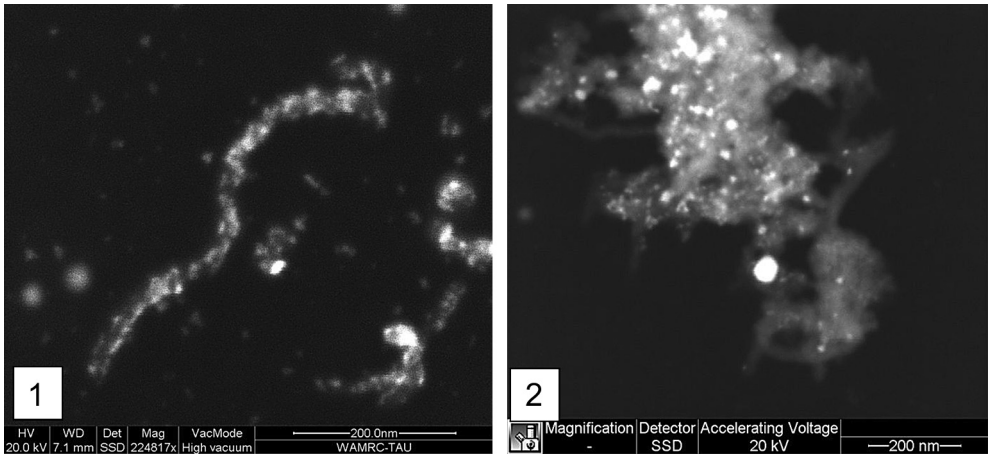


**Fig. 8.** Dark-field STEM images of tin-coated MWCNT sample (1) and the anode after cycling of Li/Sn-MWCNT cell (2).

were not destroyed by cycling. Clustering observed in the STEM image of the cycled anode is caused by the binder, as well.

## 4. Summary

Tin-based anode material supported by multiwall carbon nanotubes, Sn-MWCNT, was synthesized by a multistep electroless deposition process. First, a tin-copper alloy, $Sn_xCu_y$, was formed on the carbon nanotubes. The preparation process of the anode material, $Sn_xCu_y$-MWCNT, consists of two main stages: the electroless deposition of copper nanoparticles on activated MWCNT and then coating tin over the copper nanoparticles by replacement deposition. The result was core (Cu)–shell (Sn) structured particles. The role of the inert metal (copper) in this structure is to strengthen the structure during the processes of expansion and contraction during repeated cycling of the anode. In the later stages of the research, it was established that it is sufficient to stabilize the tin particles by the carbon nanotubes, which provide improvement of the specific capacity of the anode on prolonged cycling.

Following adjustment of the variables of the Cu/Sn replacement process, a direct electroless plating of tin nanoparticles on the activated MWCNT was developed. The final optimized product is an Sn-MWCNT anode with 11–20% higher volumetric capacity than that of the graphite anode and excellent reversible capacity stability compared to the results of other published work. This anode retains 71% of its initial reversible capacity up to the 280th cycle. In addition, the anode has a significant advantage over the graphite anode in terms of battery safety.

## Acknowledgement

We thank the Ministry of Energy and Water Resources, Israel (research grant 29-11-006/2009-7-6) for financial support of the project

## References

[1] W.J. Zhang, Journal of Power Sources 196 (2011) 13–24.
[2] A. Ulus, Yu. Rosenberg, L. Burstein, E. Peled, Journal of Electrochemical Society 149 (5) (2002) A635–A643.
[3] B. Scrosati, J. Garche, Journal of Power Sources 195 (2010) 2419–2430.
[4] G. Derrien, J. Hassoun, S. Panero, B. Scrosatti, Advanced Materials 19 (2007) 2336–2340.
[5] J. Hassoun, Y.K. Sun, B. Scrosatti, Journal of Power Sources 196 (2011) 343–348.
[6] Z.P. Gue, Z.W. Zhao, H.K. Liu, S.X. Dou, Carbon 43 (2005) 1392–1399.
[7] Y.R. Jhan, J.G. Duh, S.Y. Tsai, Diamond & Related Materials 20 (2011) 413–417.
[8] S. Yang, H. Song, H. Yi, W. Liu, H. Zhang, X. Chen, Electrochimica Acta 55 (2009) 521–527.
[9] C. Zhai, N. Du, H. Zhang, J. Yu, P. Wu, C. Xiao, D. Yang, Nanoscale 3 (2011) 1798–1801.
[10] C.L. Zhu, M. Zhang, Y. Qiao, P. Gao, Y. Chen, Materials Research Bulletin 45 (2010) 437–441.
[11] L. Huang, J. Cai, Y. He, F. Ke, S. Sun, Electrochemistry Communications 11 (2009) 950–953.
[12] I.A. Courtney, J.S. Tse, J. Hafner, J.R. Dahn, Physical Review B 58 (1998) 15,583–15,589.
[13] M. Armand, J.-M. Tarascon, Nature 451 (2008) 652–657.
[14] P.P. Ferguson, A.D.W. Todd, J.R. Dahn, Electrochemistry Communications 10 (2008) 25–31.
[15] M.R. Wagner, P.R. Raimann, A. Trifonova, K.-C. Moeller, J.O. Besenhard, M. Winter, Electrochemical and Solid-state Letters 7 (7) (2004) A201–A205.
[16] E. Perre, P.L. Taberna, D. Mazouzi, P. Poizot, T. Gustafsson, K. Edstrom, P. Simon, Journal of Materials Research 25 (8) (2010) 1485–1491.
[17] X. Chen, K. Kierzek, K. Wilgosz, J. Machnikowski, J. Gong, J. Feng, T. Tang, R.J. Kalenczuk, H. Chen, P.K. Chu, E. Mijowska, Journal of Power Sources 216 (2012) 475–481.
[18] F.M. Hassan, Z. Chen, A. Yu, Z. Chen, X. Xiao, Electrochimica Acta 87 (2013) 844–852.
[19] D. Ahn, X. Xiao, Y. Li, A.K. Sachdev, H.W. Park, A. Yu, Z. Chen, Journal of Power Sources 212 (2012) 66–72.
[20] S. Brutti, J. Hassoun, B. Scrosati, C.Y. Lin, H. Wu, H.W. Hsieh, Journal of Power Sources 217 (2012) 72e76.
[21] Y. Xu, J. Guo, C. Wang, Journal of Materials Chemistry 22 (2012) 9562.
[22] J. Hassoun, D.J. Lee, Y.K. Sun, B. Scrosati, Solid State Ionics 202 (2011) 36–39.
[23] J.W. Zheng, S.M.L. Nai, M.-F. Ng, P. Wu, J. Wei, M. Gupta, Journal of Physical Chemistry C 113 (31) (2009) 14,015–14,019.
[24] J. Wolfenstine, J. L. Allen, J. Read, D. Foster, Sensors and Electron Devices Directorate, ARL-TN-0257.
[25] H. Inoue, S. Mizutani, H. Ishihara, S. Hatake, 214th ECS Meeting, Abstract #1160.
[26] G.K. Simon, t. Goswami, Metallurgical and Materials Transactions A 42 (2011) 231.
[27] J.H. Lee, B.-S. Kong, S.B. Yang, H.-T. Jung, Journal of Power Sources 194 (2009) 520–525.
[28] W.L. Liu, S.H. Hsieh, W.J. Chen, Applied Surface Science 253 (2007) 8356–8359.
[29] Y. Kong, J. Shao, W. Wang, Q. Liu, Z. Chen, Journal of Alloys and Compounds 477 (2009) 328–332.
[30] Bath for electroless depositing tin on substrates, Patent US4269625.
[31] J.H. Byeon, Journal of Hwang Surface & Coating Technology 203 (2008) 357–363.
[32] F. Wang, S. Arai, M. Endo, Electrochemistry Communications 6 (2004) 1042–1044.
[33] Á. Caballero, J. Morales, L. Sánchezz, Electrochemical and Solid-state Letters 8-9 (2005) A464–A466.
[34] L. Noerochim, J.-Z. Wanga, S.-L. Choua, H.-J. Lib, H.-K. Liua, Electrochimica Acta 56 (2010) 314–320.
[35] J. Yu, N. Grossiord, C.E. Koning, J. Loose, Carbon 45 (2007) 618–623.
[36] Y. Wang, J. Wu, F. Wei, Carbon 41 (2003) 2939–2948.
[37] Y. Peng, Q. Chen, Colloids and Surfaces A: Physicochemical and Engineering Aspects 342 (2009) 132–135.